High performance of core type phase shifter in silicon MZM

R. G. JESUWANTH SUGESH, A. SIVASUBRAMANIAN*
School of Electronics Engineering, Vellore Institute of Technology, Chennai, 600127, India

A novel design of a core-based rib waveguide PN junction phase shifter of length 2 mm is proposed in this paper. Two PN junctions are formed on top and bottom of the core, and improved modulation efficiency is achieved. The unbalanced MZM with this proposed phase shifter is analysed for a wavelength of 1553.5 nm with the simulation results. The permissible loss of 7.8 dB occurred in this design. At 100 Gbps, an extinction ratio of 8.15 dB and bit error rate of 3.51×10^{-6} is obtained at VπL of 1V.cm. This device can be a better choice for high-speed data rate communication applications.

(Received June 29, 2020; accepted February 12, 2021)

Keywords: Silicon photonic device, Silicon Mach-Zehnder modulator, PN junction phase shifter, Optical communication system, Data centre application

1. Introduction

World's hunger for data is expanding at an alarming rate [1] with the dawn of technologies such as Cloud computing, Artificial Intelligence, Internet of Things, 5G, etc. Data centres are increasing their capacity to meet the growing demands. International Telecommunication Union (ITU) has provided the regulations (ITU-T G.671) on Dense Wavelength Division Multiplexing (DWDM) and flexible DWDM grid applications with variety and wider channel spacing, to maximum utilise the optical bandwidth. With the flexible DWDM grid policy, a mixed bit rate or mixed modulation format transmission system is possible. Silicon photonics (SiPh) uses the advanced CMOS fabrication technology to provide a cost-efficient method to transfer optical data on and off-chip. SiPh allows the integration of electronic and photonic devices on a monolithic platform [2, 3].

Electro-optic modulators play a significant role in high-speed data transmission between electronic and photonic components [4-6]. The optical modulator embeds the electrical message signal on to the carrier optical signal. The essential criteria when designing a SiPh optical modulator is that it should be of small footprint, low power consuming CMOS fabrication capable device for utilisation in a photonic integrated circuit. Micro ring resonator-based modulators provide high modulation efficiency and small footprint. They are plagued with thermal instability and require a high voltage just to maintain phase shift [7]. As a result of thermal instability, fabrication complexity and narrow bandwidth operations, micro ring resonator-based modulator's usage in on-chip applications are limited. Thermal stability, ease of fabrication and high performance make Mach Zehnder modulators (MZM) preferred among other modulators. The drawbacks in an MZM are the large footprint and power consumption [8].

Optical modulators with materials such as Indium Tin Oxide, graphene, etc. provide high modulation efficiency but are not compatible with CMOS fabrication technology as silicon [9 - 15]. Optical modulators with doped silicon are preferred as they are CMOS fabrication compatible. The modulation in silicon follows the plasma dispersion effect, where external bias voltage produces a carrier density variation which leads to index variation [16]. Two standard techniques based on the bias voltage applied are carrier injection by forward bias voltage and carrier depletion by the reverse bias voltage. High modulation efficiency (low VπL) is obtained in carrier injection technique, but it suffers from low 3dB bandwidth due to long free-carrier lifetime and high diffusion junction capacitance [4]. The carrier depletion technique overcomes this drawback, and it also supports high-speed data transmission [17, 18]. The carrier depletion technique has a disadvantage of low modulation efficiency (high VπL) due to the requirement of high reverse bias voltage (Vπ) or long transmission length (L) to obtain the required π phase shift.

The phase shifter plays a significant role in determining the performance of the optical modulator based on the doping concentration and pattern used. The phase shifters based on the doping pattern are classified into interleaved, horizontal and vertical type [19-33]. Interleaved type phase shifter provides high modulation efficiency due to multiple PN junctions along the length of the phase shifter at the cost of fabrication complexity. Vertical type phase shifters used vertical doped slabs with high carrier doping concentration. With high carrier concentration, the loss in the phase shifter increases due to free carrier absorption. The horizontal type phase shifter uses low doping concentration. Thus, the loss is less at the expense of length of the phase shifter. U shaped PN junction was designed, which provided higher optical overlap with the carrier depletion region in [27]. Higher light-matter interaction and low loss were obtained in the slot like structures in [30, 31]. Demonstrated that Silicon modulators are suited for high-speed data transmission [29]. Modulation bandwidth also influences the

modulator's efficiency. The RC time constant restricts the modulation bandwidth in lumped design, thus travelling wave (TW) electrodes are preferred. TW electrodes support carrier depletion-mode operation but have a large footprint [31–35].

A novel design of core-based rib waveguide is proposed in this paper to provide better light-matter interaction and low loss. The PN junctions are formed at the top and bottom of the core, which is driven by external reverse bias. Section II explains the device structure. The wavelength of 1553.5 nm that supports DWDM operation is selected for simulation analysis, and the results are analysed in section III. High-speed performance with a low VπL of 1V cm makes the proposed design an ideal candidate to meet the demands of the high-speed data transmission for data centre applications.

2. Device structure

Fig. 1 shows the 3D cross-sectional view of the proposed phase shifter. The phase shifter is designed over a 2 µm silicon dioxide (SiO_2) layer (Buried Oxide - BOX) on a silicon substrate of CMOS fabrication foundry standard thickness of 220 nm. The BOX reduces the coupling of the optical mode transmitted into the silicon substrate at the bottom. The rib width and the slab thickness are 500 nm and 90 nm, respectively. The thickness of the rib (t_{rib}) is 220 nm. The core width (W_x) and thickness (T_z) are 100 nm each. Fig. 2 shows the light propagation through the waveguide. By splitting the PN junctions, the capacitance and resistance of the individual junction are reduced, thus reducing the RC time constant. The optical mode interacts with the two PN junctions formed on top and bottom of the core, thus improving the light-matter interaction. The maximum mesh step is set to 50 nm and minimum to 1 pm with 1.414 as the mesh grading factor. The charge behaviour at the interface between materials where electrons and holes interact at the surface and recombine is also considered in the simulation analysis. The ion implantation doping behaviour is impersonated using a Gaussian distribution profile. The P (Boron) and N (Phosphorous) doping concentration are 9×10^{17} cm^{-3} and 7×10^{17} $cm^{-3,}$ respectively. The concentration of holes is selected higher than the concentration of electrons, as holes provide large index shift and have low absorption than electrons [16]. The P+ and N+ region are doped with concentration of 1×10^{19} cm^{-3} to reduce the excess slab resistance. Aluminium (Al) electrodes are used for electrical contacts. The carriers in the two PN junctions are depleted with the application of a voltage (reverse bias) in the cathode and the other contact is grounded. A surface oxide layer (SOX) of SiO_2 is formed at the top of the device to protect the device from external impurities.

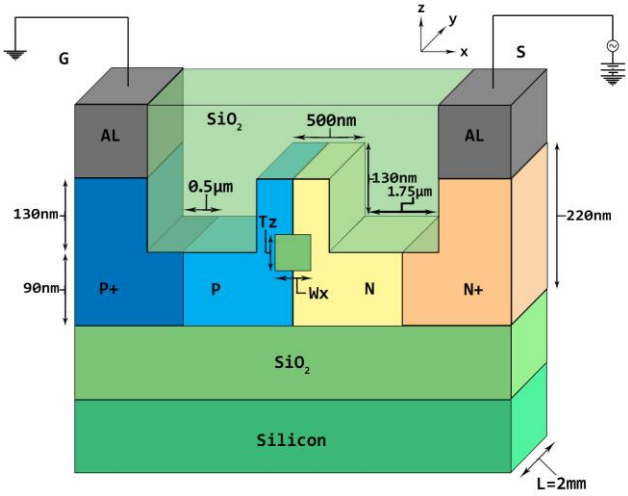

Fig. 1. Cross-sectional view of the proposed phase shifter design (The y-axis denotes the light propagation and z-axis the thickness) (color online)

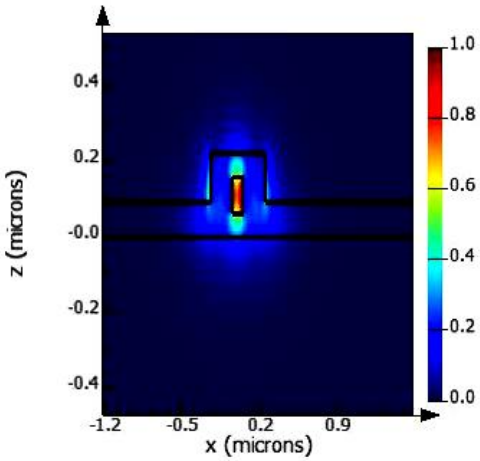

Fig. 2. Optical mode (TE_1) transmission through the waveguide (color online)

3. Result analysis

The proposed phase shifter's performance is analysed using a commercially available analytical tool [36]. The electro-optic and the RF characteristics of the phase shifter (PS) was performed using the Finite difference eigenmode (FDE) analysis in the device level simulation (Fig. 3.a). The designed phase shifter was imported into an MZM (PS-MZM), and the system-level analysis was performed in Lumerical Interconnect (Fig. 3.b). High-speed data rate and long-distance transmission analysis were also performed to analyse the PS-MZM's performance for DWDM and data centre on and off-chip transmission application.

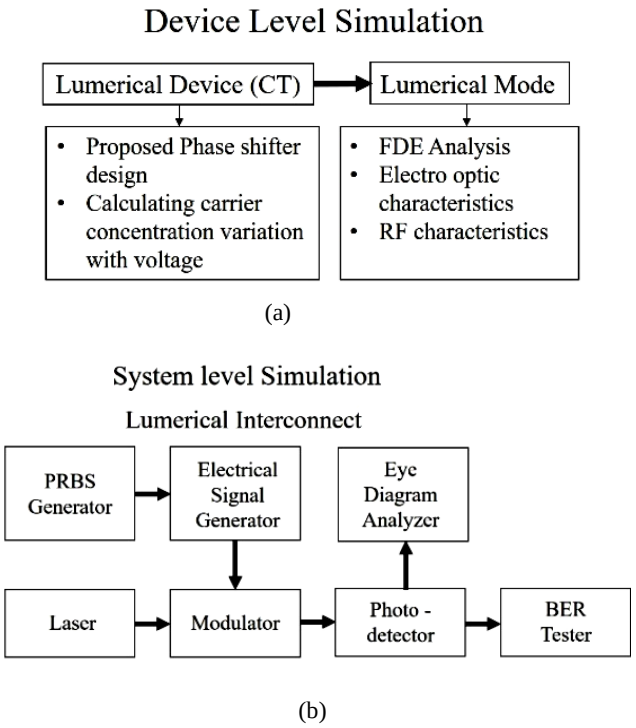

Fig. 3. Simulation flow for the analysis of the proposed phase shifter (a) Device-level simulation and (b) system-level simulation

3.1. Device-level analysis

The PS was analysed by varying the external reverse bias voltage up to a maximum of 5 V. With the increase in external reverse bias voltage, the carriers are depleted from the centre of the waveguide, as shown in Fig. 4 (a) and (b). The decrease in free carrier density causes the capacitance along the junction to reduce, as illustrated in Fig. 4.c. The capacitance of the junction is calculated (1) based on the electron (N_n) and hole (N_p) density,

$$C = \frac{t_{rib} \times \sqrt{(q\,\varepsilon_o\,\varepsilon_r)}}{\sqrt{(2(N_p^{-1} + N_n^{-1}) \times (V_v - V))}} \quad (1)$$

where q denotes the electric charge, ε_0 the dielectric constant, ε_r the relative permittivity and V_v the diffusion potential.

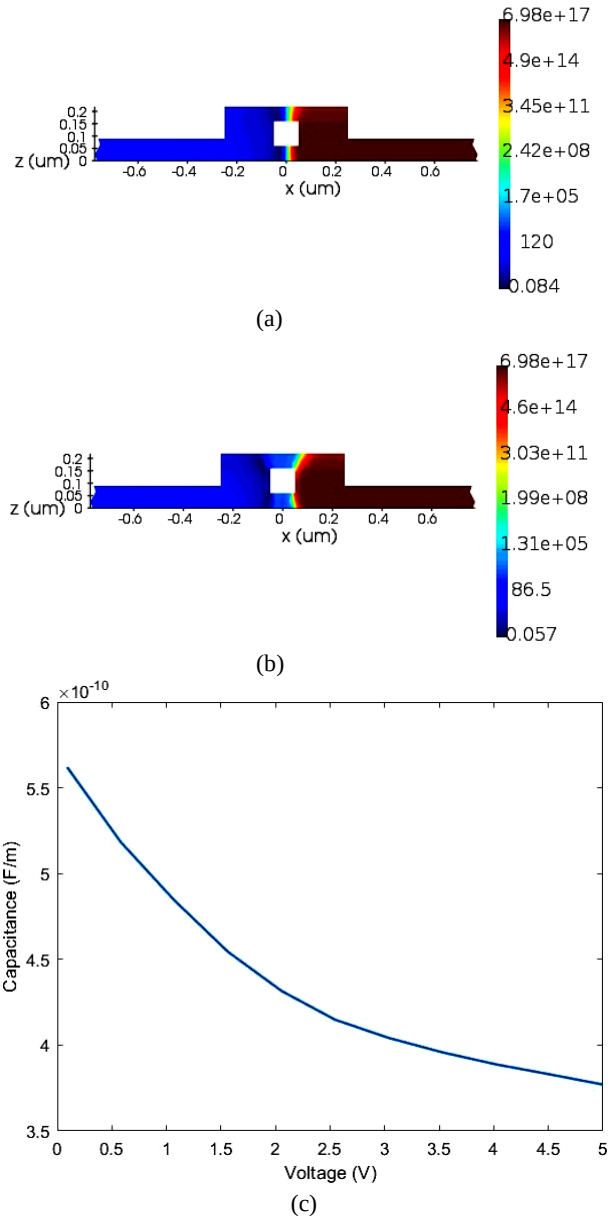

Fig. 4. (a) Electron depletion with respect to voltage at V = -0.5V and (b) V = -3.5V. (c) Capacitance measured in the PN junctions with respect to reverse bias voltage (color online)

The depletion of carriers in the PS influences the refractive index (Δn) and the absorption coefficient (Δα) of the PS. Soref and Bennett derived the mathematical relationship of (2) and Δα (3) on free carrier density based on experiments [16]. In the proposed design, the core splits the PN junction into two junctions. This increases the interaction of the optical mode with the depletion region and further adds to the refractive index change with respect to voltage.

$$\Delta n = -8.8 \times 10^{-22} N_n - 8.5 \times 10^{-18} N_p^{\,0.8} \quad (2)$$

$$\Delta\alpha = 8.5 \times 10^{-18} N_n + 6 \times 10^{-18} N_p \quad (3)$$

The effective index change with voltage ($\Delta n_{eff}(V)$) alters the optical property of the PS. This causes a phase

shift (φ) on the propagating optical wave along the PS length (L), which is calculated by (6).

$$n_{eff}(V) = n_{eff,i} + \int \Delta n(V) dV \quad (4)$$

where, $n_{eff,i}$ denotes the effective index of the waveguide without doping.

$$\Delta n_{eff}(V) = n_{eff}(V) - n_{eff}(0) \quad (5)$$

$$\varphi(V) = \frac{2\pi \Delta n_{eff}(V) L}{\lambda} \quad (6)$$

The absorption coefficient α along the PS (z-axis) is obtained from (7).

$$\alpha(z) = \frac{\iint \Delta\alpha(V)|E(x,y,z)^2|dxdy}{\iint |E(x,y,z)^2|dxdy} \quad (7)$$

where, x, y denotes the waveguide dimension coordinates, and z denotes the length coordinate of the PS, and E(x,y,z) the optical intensity distribution of the waveguide mode.

The carrier depletion with voltage reduces the interaction of the carriers with the propagating optical wave. Photons get absorbed by the carriers (free carrier absorption loss), and thus the core with width W_x = 100 nm and thickness T_z = 100 nm is preferred. The core provides optical confinement, reduces the absorption of photons by carriers and also helps to obtain the required π phase shift for optical modulation. The phase shift required is obtained at a reverse bias voltage of 5 V (Vπ) in the proposed design for 2 mm PS length with a loss of 2.33 dB. The variation of Vπ along with the loss as a function of the PS length in shown in Fig. 5. It is observed that as L increases the Vπ reduces as the propagating optical wave is exposed to the phase shift change throughout the phase shifter length. But as the interaction of the carriers with optical mode is increased with length, the loss increases with L. The absorption loss is the dominant loss in the PS and can be further reduced by increasing the core dimension at the expense of Vπ. Fabrication imperfectness or roughness along the waveguide side walls also add to the losses in the PS which can be reduced by optimizing the etching process.

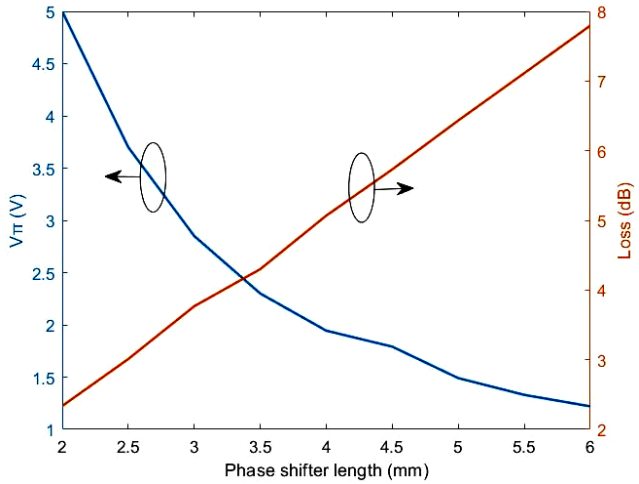

Fig. 5. Vπ and Loss variation with respect to phase shifter length for the proposed design (W_x = T_z= 100 nm) (color online)

At ideal conditions, the 3dB intrinsic bandwidth ($f_{3dB} = \frac{1}{2\pi RC}$) of the proposed phase shifter is calculated. The intrinsic bandwidth of the PS is inversely proportional to the length. In order to overcome the RC time constant and to tightly couple the RF microwave wave with the optical wave, a travelling wave electrode is used. For strong coupling between the RF and optical wave at higher microwave frequencies, the optical group index (OGI) has to be minimum. The OGI variation with the design parameters is shown in Fig. 6. It is observed that the minimum OGI value of 3.43 is obtained and reducing the core dimensions will reduce OGI value at the cost of Vπ. Thus, core with width W_x= 100 nm and thickness T_z = 100 nm is preferred. At 52 GHz, the RF effective index is matched to the OGI value, and strong coupling occurs (Fig. 7). At 52 GHz, 6 dB loss is acquired as shown in Fig. 7, and it is witnessed that loss is directly proportional to microwave frequency. 6 dB bandwidth of 32 GHz is attained for the designed structure of length 2 mm (Fig. 8) and ensures that the device can be utilized for high-speed data rate communication applications.

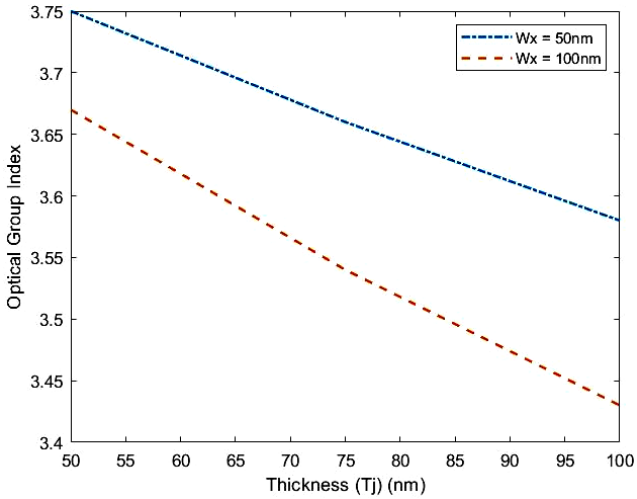

Fig. 6. Variation of Optical group index based on design parameters of the core width (W_x) and core thickness (T_z) (color online)

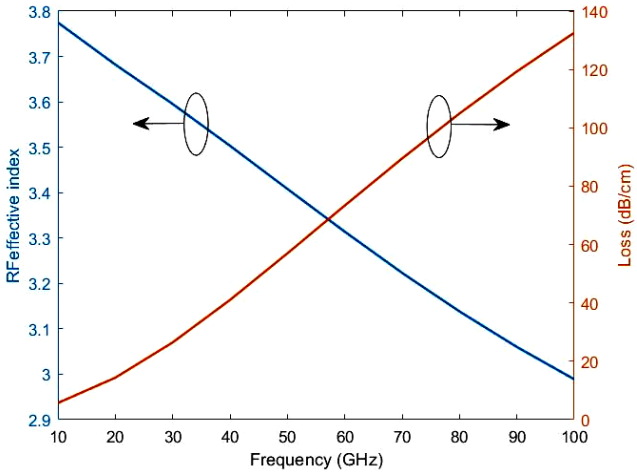

Fig. 7. RF effective index and Loss acquired with respect to frequency (color online)

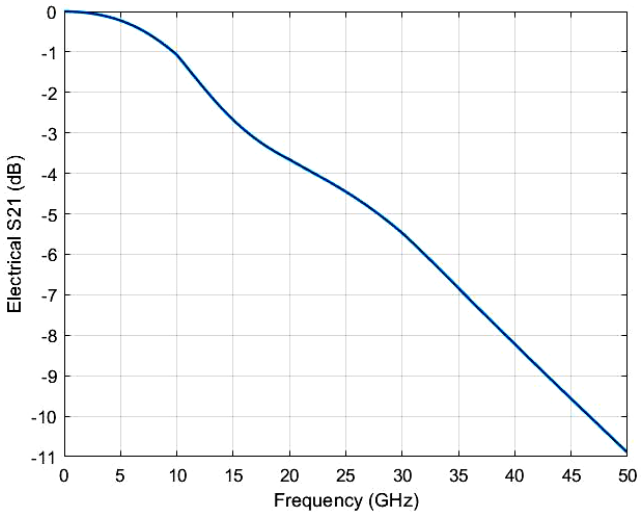

Fig. 8. Electrical S21 (dB) with respect to frequency

3.2. System-level analysis

The dynamic performance of an unbalanced MZM incorporated with the designed PS (PS-MZM) is studied. The PS-MZM has an intentional length variation of 100 µm with longer arm provided a fixed bias voltage of 1V and an alternating voltage swing (V_{pp}) with DC bias (V_{dc}) is applied to the other arm. The message data is generated from a pseudo-random bit sequence (PRBS) generator at 100 Gbps. The message data is then converted to a message signal by an NRZ line coder electrical signal generator. The message signal is modulated on an optical carrier signal of 1553.5 nm generated by CW Laser. The optical signal is demodulated by the PIN photodetector with a responsivity of 1 A/W. An eye diagram analyser and a bit error rate (BER) tester are used for analysing the obtained signal. At 5 V_{pp} and 1 V_{dc}, an eye diagram (Fig. 9) with ER of 8.15 dB and BER of 3.51×10^{-6} was obtained for a VπL of 1V.cm. The eye-crossing at around 50% and wide eye opening leads to minimum duty cycle distortion and low inter-symbol interference. This ensures that PS-MZM is suitable for high speed data rate applications. The energy per bit utilization ($E_{bit} = \frac{CV^2}{4}$) for the data transmission is calculated to be 4.7 pJ/bit. The performance of the PS-MZM is compared with the results of published articles with depletion type MZM in Table 1.

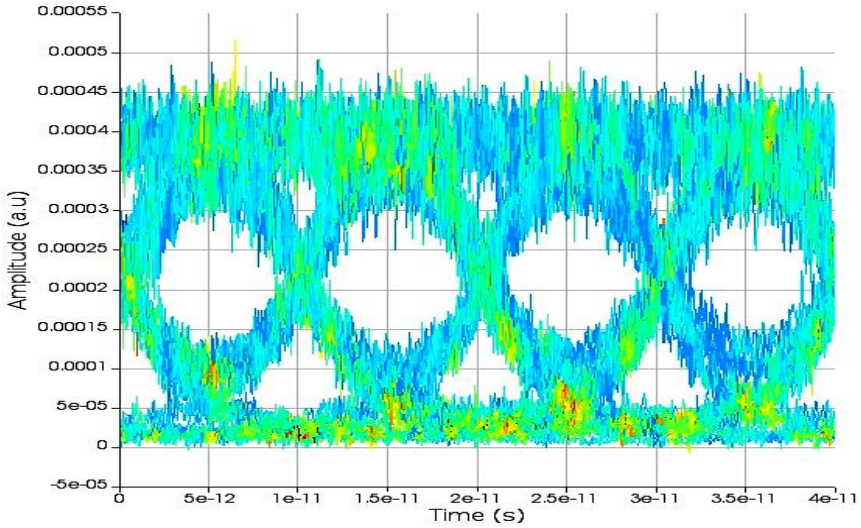

Fig. 9. Eye diagram for PS-MZM with VπL = 1V.cm (color online)

Table 1. Parameter comparison with published results

Ref	L (mm)	Gbps	VπL (V.cm)	ER (dB)
[20]	0.75	40	1.5	7.01
[21]	8	-	3.1	18
[22]	3	10	1.08	11
[23]	2	24	0.46	2.2
[26]	1.5	112	2.3	-
[28]	2	40	1.8	8
[29]	5	100	2.5	5
[31]	1.2	100	0.74	2.4
[32]	1.8	40	0.54	14.5
This work	2	100	1	8.15

In [20], high voltage was used in a short phase shifter to obtain the same ER. Higher ER was obtained in [21] by increasing the length of the phase shifter. In [29], the phase shifter of length 5 mm is used to obtain the π phase shift with an ER of 5.5 dB. The length was reduced to 1.2 mm [31], but a reverse bias voltage of around 6V is required, and 2.4 dB of ER was obtained. Higher ER was obtained in [32] but was restricted to 40 Gbps. From Table 1, it is clear that designed phase shifter in MZM performs better when compared with other published results.

Intra data centre communication range till 10 km by optical fibre cables. The performance of PS-MZM for off-chip communication is analysed by placing an optical fibre cable with attenuation of 0.2 dB/km before the PIN

photodetector. At 100 Gbps, long-distance transmission performance is analysed for PS-MZM. It is observed from Fig. 10 that BER is proportional to length. It is inferred that the forward error correction (FEC) threshold of BER rate 1×10^{-3} (between chips) is reached at 18 Km. This ensures the PS-MZM can be utilised for guided wave transmission (optical fibre) and unguided wave transmission (free space optics) in intra data centre application. The transmission length can be increased with a filter or amplifier.

The bit rate analysis for PS-MZM is studied by varying the bit rate, and BER is calculated. With the increase in bit rate, BER increases as inferred from Fig. 11. It is observed that PS-MZM supports up to 125 Gbps. The bit rate support can be improved by increasing the PIN photodetector's responsivity or introducing an amplifier.

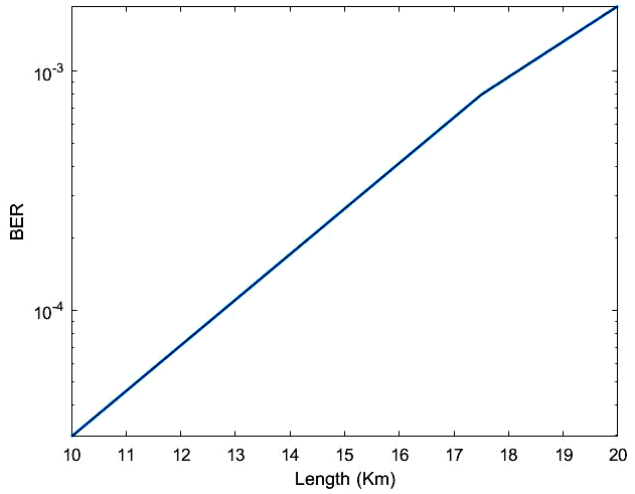

Fig. 10. PS-MZM's performance for distance transmission without amplifier at VπL of 1 V.cm

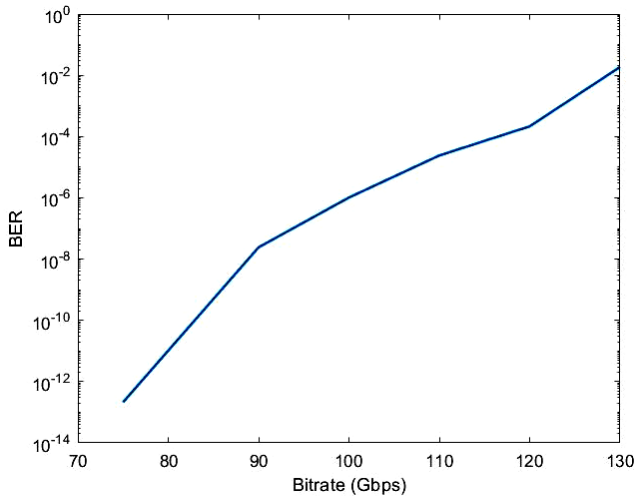

Fig. 11. PS-MZM's performance for bit rate at VπL of 1 V.cm

4. Conclusion

A core-based rib waveguide PN junction phase shifter of length 2 mm designed for high data rate data centre applications is discussed in this paper. This novel design has two PN junctions on the top and bottom of the core (W_x = T_z = 100 nm). The carriers are depleted by applying reverse bias voltage, and better modulation efficiency was achieved. It also improved the coupling between the optical mode and RF mode with the TW electrode. The confinement within the core region allowed the velocity matching between the RF and optical mode. At a low VπL of 1 V.cm, an intrinsic bandwidth of 42.6 GHz was obtained (without TW electrode). The designed phase shifter with an unbalanced MZM (PS-MZM), and the simulation analysis was performed. As per ITU-T G.671 recommendation for DWDM application, the carrier signal wavelength was set to 1553.5 nm. At 100 Gbps, an ER of 8.15 dB and BER of 3.51×10^{-6} was obtained at VπL of 1 V.cm with energy per bit of 4.7pJ/bit. The FEC threshold reached at 125 Gbps when analysing the speed performance of PS-MZM for on-chip and 18 Km at 100 Gbps for off-chip transmission. This ensures that PS-MZM is an ideal candidate for intra and inter-data centre DWDM application. The proposed device also finds other applications such as optical switches, delay lines, free space optics etc.

Acknowledgments

Authors thank Vellore Institute of Technology, Chennai for providing support and resources for this work.

References

[1] Cisco Annual Internet Report (2018–2023) White Paper. [Online] Available: https://www.cisco.com/c/en/us/solutions/collateral/service-provider/visual-networking-index-vni/white-paper-c11-741490.html.

[2] H. Subbaraman, X. Xu, A. Hosseini, X. Zhang, Y. Zhang, D. Kwong, R .T. Chen, Opt. Express **23**(3), 2487 (2015).

[3] D. Thomson, A. Zilkie, J. E. Bowers, T. Komljenovic, G. T. Reed, L. Vivien, D. Marris-Morini, E Cassan, L. Virot, J. M. Fédéli, J. M. O'Brien, G. Z. Mashanovich, M. Nedeljkovic, J. Opt. **18**(7), 073003 (2016).

[4] Q. Xu, S. Manipatruni, B. Schmidt, J. Shakya, M. Lipson, Conf. Lasers Electro-Optics, CLEO 2007, **15**, 430 (2007).

[5] W. M. Green, M. J. Rooks, L. Sekaric, Y. A. Vlasov, Opt. Express **15**(25), 17106 (2007).

[6] L. Chen, K. Preston, S. Manipatruni, M. Lipson, Opt. Express **17**(17), 15248 (2009).

[7] F. Y. Gardes, A. Brimont, P. Sanchis, G. Rasigade, D. Marris-Morini, L. O'Faolain, F. Dong, J. M. Fedeli, P. Dumon, L. Vivien, T. F. Krauss, G. T. Reed, J.

Martí, Opt. Express **17**(24), 21986 (2009).
[8] R. G. Jesuwanth Sugesh, A. Sivasubramanian, Lect. Notes Electr. Eng. **468**, 185 (2018).
[9] L. Alloatti, R. Palmer, S. Diebold, K. P. Pahl, B. Chen, Dinu R. M. Fournier, J. M. Fedeli, T. Zwick, W. Freude, C. Koos, J. Leuthold, Light Sci. Appl. **3**, 173 (2014).
[10] N. Youngblood, Y. Anugrah, R. Ma, S. J. Koester, M. Li, Nano Lett. **14**(5), 2741 (2014).
[11] X. Zhang, C. Chung, A. Hosseini, H. Subbaraman, J. Luo, A. K.-Y. Jen, R. L. Nelson, C. Y.-C. Lee, R. T. Chen, J. Light Technol. **34**(12), 2941 (2016).
[12] J. Baek, J.-B. You, K. Yu, Opt. Express **23**(12), 15863 (2015).
[13] H. Dalir, Y. Xia, Y. Wang, X. Zhang, ACS Photonics, **3**(9),1564 (2016).
[14] S. Rajput, V. Kaushik, S. Jain, M. Kumar, IEEE Photonics J. **11**(1), 1 (2019).
[15] S. Rajput, V. Kaushik, S. Jain, P. Tiwari, A.K. Srivastava, M. Kumar, J. Light Technol. **38**(6), 1365 (2020).
[16] R. Soref, B. Bennett, IEEE J. Quantum Electron. **23**(1), 123 (1987).
[17] A. Liu, L. Liao, D. Rubin, H. Nguyen, B. Ciftcioglu, Y. Chetrit, N. Izhaky, M. Paniccia, Opt. Express **15**(2), 660 (2007).
[18] M. Ziebell, D. Marris-Morini, G. Rasigade, J-M. Fédéli, P. Crozat, E. Cassan, D. Bouville, L. Vivien, Opt. Express **20**(10), 10591 (2012).
[19] P. Dong, L. Chen, Y. Chen, Opt. Express **20**(6), 6163 (2012).
[20] H. Xu, X. Xiao, X. Li, Y. Hu, Z. Li, T. Chu, Y. Yu, J. Yu, Opt. Express **20**(14), 15093 (2012).
[21] A. Rao, A. Patil, P. Rabiei, A. Honardoost, R. DeSalvo, A. Paolella, S. Fathpour, Opt. Lett. **41**(24), 5700 (2016).
[22] K. Ogawa, K. Goi, N. Ishikura, H. Ishihara, S. Sakamoto, T-Y. Liow, X. Tu, G-Q. Lo, D-L. Kwong, S. T. Lim, M. J. Sun, C. E. Png, Proc. SPIE Opto. **9752**, 975202 (2016).
[23] Z. Yong, W. D. Sacher, Y. Huang, J. C. Mikkelsen, Y. Yang, X. Luo, P. Dumais, D. Goodwill, H. Bahrami, P. G. Q. Lo, E. Bernier, J. K. S. Poon, OFC Conf., OSA, Tu2H-2, (2017).
[24] M. F. Rosa, L. Rathgeber, R. Elster, N. Hoppe, T. Föhn, M. Schmidt, W. Vogel, M. Berrot, Adv. Radio Sci. **15**, 269 (2017).
[25] T. Y. L. Ang, C. E. Png, S. T. Lim, Proc. Silicon Photonics XII **10108**, 1010804 (2017).
[26] G. B. de Farias, Y. R. Bustamante, H. A. de Andrade, U. C. Moura, A. P. Freitas, D. de A. Motta, 2018 IEEE 15th Int. Conf. Gr. IV Photonics 1 (2018).
[27] Z. Yong, W. D. Sacher, Y. Huang, J. C. Mikkelsen, Y. Yang, X. Luo, P. Dumais, D. Goodwill, H. Bahrami, P. G.-Q. Lo, E. Bernier, J. K. S. Poon, Opt. Express **26**(25), 32757 (2018).
[28] C. Wang, M. Zhang, B. Stern, M. Lipson, M. Lončar, Opt. Express **26**(2), 1547 (2018).
[29] M. He, M. Xu, Y. Ren, J. Jian, Z. Ruan, Y. Xu, S. Gao, S. Sun, X. Wen, L. Zhou, C. Guo, H. Chen, S. Yu, L. Liu, X. Cai, Nat. Photonics **13**, 359 (2019).
[30] S. Jain, S. Rajput, V. Kaushik, M. Kumar, Opt. Commun **434**, 49 (2019).
[31] S. Jain, S. Rajput, V. Kaushik, Sulabh, M. Kumar, IEEE J. Quantum Electron. **56**(2), 1 (2020).
[32] M. Makarov, M. Barabanenkov, A. Italyantsev, Photonics North (PN) **1**, 1 (2020).
[33] T. Baehr-Jones, R. Ding, Y. Liu, A. Ayazi, T. Pinguet, N. C. Harris, M. Streshinsky, P. Lee, Y. Zhang, A. E.-J. Lim, T.-Y. Liow, S. H.-G. Teo, G.-Q. Lo, M. Hochberg, Opt. Express **20**(11), 12014 (2012).
[34] J. P. Dakin, R. G. Brown, "Handbook of Optoelectronics (two-volume set)", CRC Press, New York, 2006.
[35] L. N. Binh, "Optical multi-bound solitons", CRC Press, London, 2015.
[36] Lumerical software. [Online] Available: https://www.lumerical.com/products/.

*Corresponding author: sivasubramanian.a@vit.ac.in